ACS OMEGA

Article

Cite This: ACS Omega 2019, 4, 6737−6745

http://pubs.acs.org/journal/acsodf

Azulicorrole

Simon Larsen,[†] Laura J. McCormick-McPherson,[‡] Simon J. Teat,[‡] and Abhik Ghosh*[,†]

[†]Department of Chemistry, UiT—The Arctic University of Norway, N-9037 Tromsø, Norway

[‡]Advanced Light Source, Lawrence Berkeley National Laboratory, Berkeley, California 94720-8229, United States

Supporting Information

ABSTRACT: Acid-catalyzed condensation of pyrrole, 4-trifluoromethylbenzaldehyde, and azulene, followed by DDQ oxidation, has resulted in the isolation of the novel macrocycle azulicorrole, arguably the first example of a carbacorrole aside from N-confused corrole. Despite poor yields (<1%), the free ligand could be structurally characterized and converted to the formal Cu(III) and Au(III) derivatives, of which the Cu(III) complex could also be structurally characterized. Both the free base and the two metal complexes exhibit richly structured UV−vis spectra that extend well into the near-infrared, suggesting potential applications in bioimaging and photodynamic therapy.

1. INTRODUCTION

Over the last quarter century, pyrrole−aldehyde condensations have served as a prolific wellspring of new porphyrinoid macrocycles, including N-confused porphyrins, corroles, sapphyrins, and both expanded and contracted porphyrins.[1−3] An even wider range of macrocycles is potentially obtainable by including reactive arenes in the reaction mixture, as exemplified by the synthesis of an azuliporphyrin[4,5] under Lindsey[6,7] conditions. Both N-confused porphyrins[8] and azuliporphyrins[9] are pre-eminent members of the carbaporphyrinoid family and give rise to a wide range of organometallic complexes.[10,11] As long-time practitioners of corrole chemistry,[12] we were intrigued by the possibility that carbacorroles[13] might arise in the course of quasi-one-pot condensation−oxidation protocols.

As shown in Chart 1, both regioisomers of a simple carbacorrole feature an exceedingly crowded central cavity with four central hydrogens. Carbacorrole variants such as N-confused corrole and the as yet experimentally unknown azulicorrole partially alleviate such crowding by incorporating only three central nitrogens. In an exploratory computational study of the two Au azulicorrole regioisomers,[14] isomer A was found to be more stable by about 2.7 kcal/mol. Herein, we describe for the first time the isolation of a free-base azulicorrole and its complexation with Cu and Au. Although the compounds are only available in milligram quantities, we were able to accomplish two single-crystal X-ray structure determinations as well as ^{1}H NMR and UV−vis measurements, which yielded some of the first insights into the properties of the novel macrocycle.

Chart 1. Selected Free-Base Carbaporphyrinoids

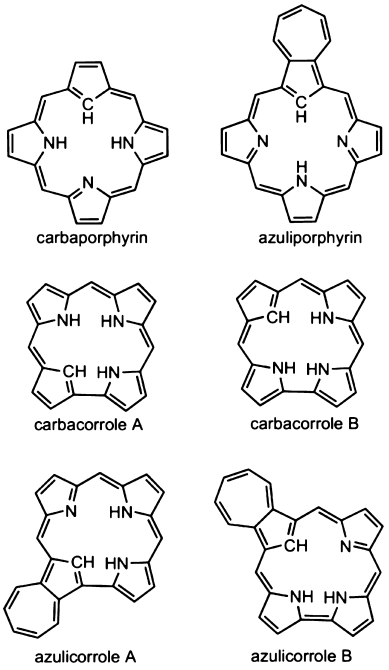

2. RESULTS AND DISCUSSION

2.1. Synthesis and Proof of Composition. Our early attempts at finding new routes to azuliporphyrinoids were

Received: January 30, 2019
Accepted: March 27, 2019
Published: April 12, 2019

DOI: 10.1021/acsomega.9b00275
ACS Omega 2019, 4, 6737−6745

thwarted by the immediate formation of calix[4]azulenes via acid-catalyzed condensation of azulene and various aromatic aldehydes. Thus, adding azulene to Gryko's "water–methanol" protocol led to calix[4]azulenes as the main isolable product. To our pleasant surprise, adding azulene to the reaction mixture of a standard solvent-free, trifluoroacetic acid (TFA)-catalyzed corrole synthesis[15−17] resulted in mass spectrometric evidence for the formation of a *meso*-triarylazulicorrole, hereafter abbreviated as H_3[AzuC] (Scheme 1). Upon careful

Scheme 1. One-Pot Synthesis of a Free-Base Azulicorrole, H_3[AzuC]

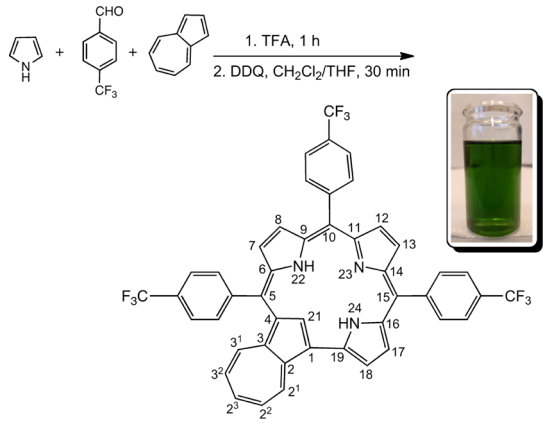

optimization of the relative amounts of pyrrole, aldehyde, azulene, and DDQ, we were finally able to isolate the pure compound, albeit in disappointingly low yields (<1%). Substantial amounts of *meso*-triarylcorrole were also isolated, along with a large quantity of azulene–aldehyde oligomers, which were not characterized in detail. Fortunately, free-base H_3[AzuC] could be readily derivatized to the formal copper(III) and gold(III) complexes.

Besides high-resolution electrospray ionization (HR-ESI) mass spectra, proof of composition also came from fully assigned ^{1}H NMR spectra in $CDCl_3$ (Figure 1). The azulene-2^1 doublet at ∼9.0−9.3 ppm is well separated from other signals and is also the only nonpyrrole proton that couples with a pyrrole β proton (at C18). Once these two protons were identified, all others could be assigned by a combination of TOCSY and nuclear Overhauser enhancement spectroscopy analyses (see the Supporting Information for detail). Unfortunately, ^{13}C NMR spectra of acceptable quality could not be obtained because of the limited solubility of the compounds.

2.2. Single-Crystal X-ray Structures. Unambiguous proof of the structure came from two single-crystal X-ray structures (Table 1), one for H_3[AzuC] (Figure 2) and the other for Cu[AzuC] (Figure 3). The azulene moiety in the free-base structure was found to be distinctly tilted relative to the remainder of the macrocycle, clearly a reflection of the steric interactions among the three central hydrogens. For the two symmetry-unique H_3[AzuC] molecules, the azulene ten-carbon plane was found to be tilted by 36.56(3) and 40.90(2)° relative to the mean $C_{15}N_3$ plane of the remainder of the macrocycle. In contrast, an essentially planar macrocycle, including an in-plane Cu atom, was found for Cu[AzuC]. The short Cu−N/C bond lengths (1.86−1.90 Å) are similar to those observed for Cu corroles.[18−24] Scalar-relativistic DFT geometry optimization (OLYP-D3/ZORA-STO/TZ2P; see ref 14 for details) of unsubstituted Au azulicorrole also indicated a rigorously planar macrocycle with short Au−N/C distances: Au−C21 1.980, Au−N22 2.021, Au−N23 2.040, and Au−N24 2.013 Å.

Careful examination of the individual skeletal bond distances in H_3[AzuC] and Cu[AzuC] revealed interesting differences in bond-length alternation between the two compounds. Thus, while H_3[AzuC] shows relatively little bond-length alternation in the seven-membered ring and significantly larger bond-length alternation in the inner fifteen-membered $C_{12}N_3$ ring of the carbacorrole, the reverse is observed for Cu[AzuC]. This observation appears to argue for a comparatively higher tropylium character in the free base relative to the Cu complex and higher macrocyclic aromaticity (i.e., a higher global diatropic current) in the Cu complex relative to the free base. Such a conclusion is in line with calculated magnetically induced current intensity patterns of porphyrinoids, particularly carbaporphyrinoids, and their metal complexes.[14]

Another interesting observation concerns the strict planarity of the macrocycle in Cu[AzuC], which may be contrasted with the invariably saddled geometry of Cu corroles. Several lines of evidence indicate that saddling in Cu corroles is driven by a $Cu(d_{x^2-y^2})$−corrole(π) orbital interaction, which imparts substantial Cu^{II}−corrole$^{\bullet 2-}$ character to the complexes.[12,18−24] The stronger σ-donor character of the azulicorrole ligand in contrast appears to stabilize a d^8 Cu(III) center in square planar environment, a scenario that is also indicated for Cu N-confused corrole by X-ray absorption spectroscopic measurements.[25] It may be worth noting in this connection that strong saddling is not observed for Au corroles, presumably reflecting the high energy of the relativistically destabilized $Au(5d_{x^2-y^2})$ orbital, which discourages effective interaction with the corrole π orbital in question.[26−30]

2.3. Electronic-Structural Insights. Standard physical measurements have afforded significant insights into key electronic-structural characteristics of the azulicorrole macrocycle.

The ^{1}H NMR spectrum of H_3[AzuC] in $CDCl_3$ revealed β-protons resonating in the range 7.21−7.95 ppm and core protons resonating at 3.19 (CH) and 3.47 ppm (NH). For the analogous *meso*-triarylcorrole, the β-H's resonate between 8.37 and 8.73 ppm and NH's between −2.0 and −4.5 ppm.[31] These chemical shifts clearly indicate a significantly lower global diatropic current for H_3[AzuC] relative to aromatic porphyrins and corroles.

To find evidence for a significant tropylium character for H_3[AzuC], we measured the ^{1}H NMR spectrum of H_3[AzuC] in solvents of different polarities, including benzene-d_6, $CDCl_3$, and DMSO-d_6. Unfortunately, low solubility hampered the assignment of the spectra in benzene or dimethyl sulfoxide (DMSO), so we could only compare the chemical shifts of some of the azulene protons across different solvents. Thus, the azulene-2^1 proton was found to move from 8.97 ppm in benzene-d_6 to 9.3 ppm in $CDCl_3$ and to 9.51 ppm in DMSO-d_6, respectively. In the same vein, the azulene triplets range between 6.29 and 6.81 ppm in benzene-d_6 and between 7.09 and 7.59 ppm in $CDCl_3$, while a single triplet was observed in DMSO at 7.92 ppm. The downfield shifts of the azulene protons with increasing solvent polarity appear to be consistent with a significant tropylium character of the seven-membered ring, as in the dipolar resonance form depicted in Scheme 2.

DOI: 10.1021/acsomega.9b00275
ACS Omega 2019, 4, 6737−6745

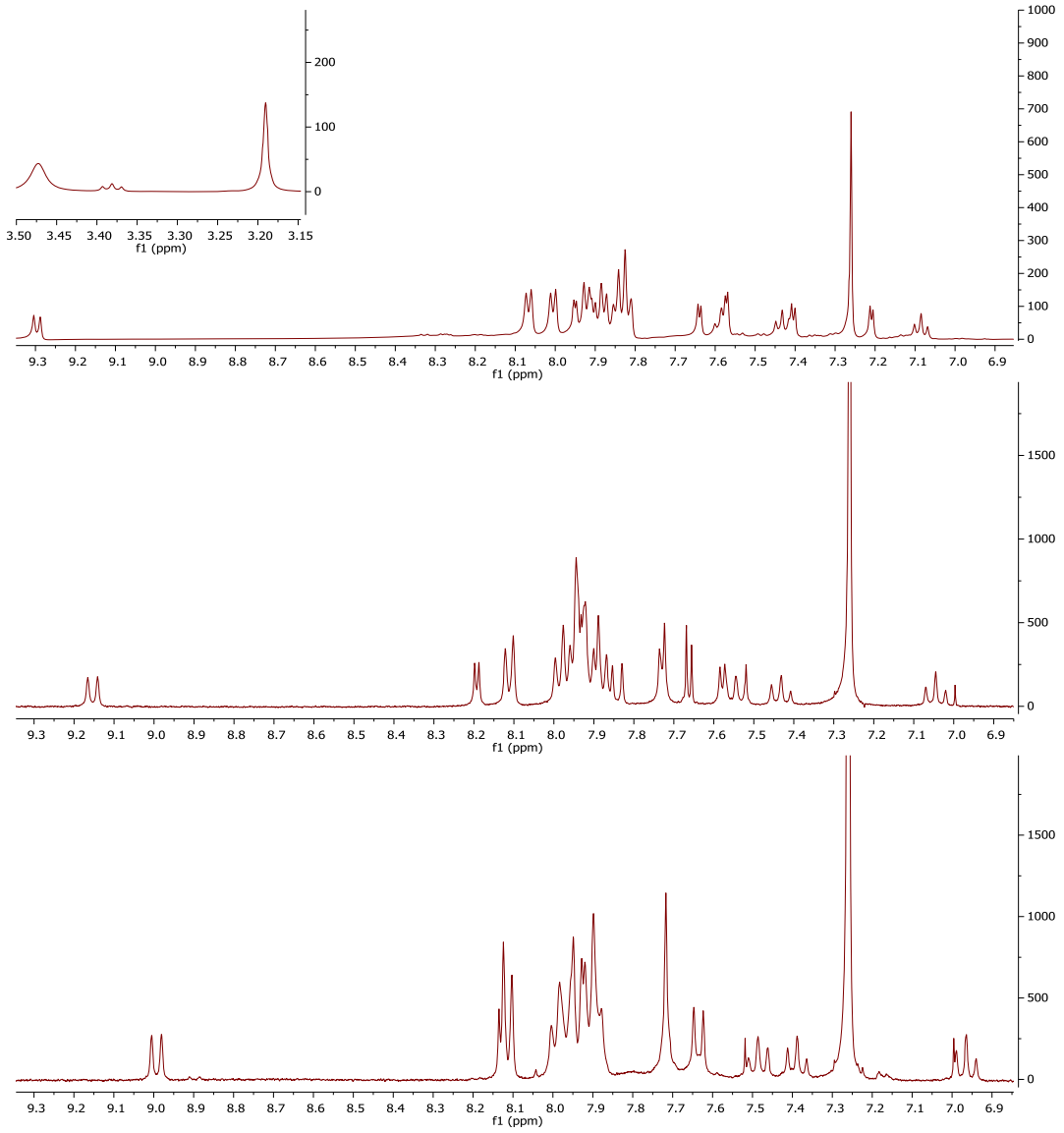

Figure 1. ^{1}H NMR spectra in $CDCl_3$ for H_3[AzuC] (top; inset displays core protons), Cu[AzuC] (middle), and Au[AzuC] (bottom).

The optical spectra of the new compounds (Figures 4–6) proved complex and richly structured, with absorption features extending well into the near-infrared (850–900 nm), suggesting a highest occupied molecular orbital–lowest unoccupied molecular orbital (HOMO–LUMO) gap of around 1.5 eV. In particular, the UV–vis–NIR spectrum of H_3[AzuC] was found to undergo dramatic changes upon exposure to TFA, with the growth of new, intense NIR features. The new features indicate a lowering of the HOMO–LUMO gap, consistent with a strongly nonplanar macrocycle, as expected for the centrally tetraprotonated macrocycle, $\{H_4[AzuC]\}^+$. Unfortunately, a ^{1}H NMR analysis of this species proved impossible because of tremendous peak broadenings.

Electrochemical measurements led to complex cyclic voltammograms (CV) for the free-base and Cu derivatives with a multitude of irreversible features that are yet to be assigned. Fortunately, Au[AzuC] yielded relatively simple CV (Figure 7) including reversible oxidation, irreversible two-electron reduction, and an electrochemical HOMO–LUMO gap (1.63 eV) in fair agreement with that estimated from the optical spectrum. Unsurprisingly, this HOMO–LUMO gap is significantly smaller than that of an Au triarylcorrole (~2.2 V),[27,28] consistent with the complex cross-conjugated nature of the azulicorrole ring system. According to the aforementioned DFT calculations, the HOMO and HOMO − 1 of unsubstituted Au azulicorrole resemble the a_{2u} and a_{1u} HOMOs of typical closed-shell porphyrins and corroles;[32−34] the LUMO and LUMO + 1, on the other hand, have considerable azulene character (Figure 8). Calculations on cationic and anionic states of the compound also clearly assigned them as pure π-radical states (Figure 8); the electrochemical HOMO–LUMO gap thus appears to correspond to the π–π^* gap of the azulicorrole macrocycle.

3. CONCLUSIONS

Adding azulene to a standard solvent-free corrole synthesis led to the isolation of an azulicorrole, arguably the first example of a "true" carbacorrole with the exception of N-confused corroles. In spite of poor yields, the free ligand could be readily derivatized to formal Cu(III) and Au(III) complexes. Furthermore, single-crystal X-ray structures could be obtained

DOI: 10.1021/acsomega.9b00275
ACS Omega 2019, 4, 6737–6745

Table 1. Crystallographic Data for H_3[AzuC] and Cu[AzuC]

sample	H_3[AzuC]·benzene	Cu[AzuC]·toluene
chemical formula	$C_{98}H_{58}F_{18}N_6$	$C_{49.50}H_{27}CuF_9N_3$
formula mass	1661.50	898.28
crystal system	monoclinic	monoclinic
crystal size (mm^3)	0.260 × 0.030 × 0.010	0.100 × 0.090 × 0.040
space group	$P2_1/n$	$P2_1/c$
λ (Å)	0.7288	0.7288
a (Å)	17.1182(19)	17.5930(12)
b (Å)	15.1767(17)	18.0587(12)
c (Å)	30.383(3)	11.9975(8)
α (deg)	90	90
β (deg)	99.8990(10)	96.358(2)
γ (deg)	90	90
Z	4	4
V ($Å^3$)	7775.8(15)	3788.2(4)
temperature (K)	100(2)	100(2)
density (g/cm^3)	1.419	1.575
measured reflections	163 422	122 388
unique reflections	23 766	9430
parameters	1135	624
restraints	24	91
R_{int}	0.0618	0.0557
θ range (deg)	1.543−31.419	2.313−29.145
R_1, wR_2 all data	0.0835, 0.1895	0.0516, 0.1159
S (GooF) all data	1.054	1.028
max/min res. dens. ($e/Å^3$)	0.753/−0.624	1.498/−0.537

for the free-base and Cu(III) derivatives, affording detailed insights into the structural characteristics of these compounds. The optical spectra proved richly structured, with absorption features extending well into the near-infrared region. Current efforts in our laboratory are aimed at uncovering higher-yielding routes toward azulicorroles with different *meso*-substituents. Should these efforts prove successful, applications vis-à-vis bioimaging and photodynamic therapy remain an exciting possibility.[35,36]

4. EXPERIMENTAL SECTION

4.1. Materials. All reagents, except pyrrole, were purchased from Sigma-Aldrich and used as received. Pyrrole was passed through basic alumina until blank and stored in the freezer. Aluminium oxide 60, active basic activity I (0.063−0.200 mm particle size, 70−230 mesh, Merck), and silica gel 60 (0.04−0.063 mm particle size, 230−400 mesh, Merck) were employed for flash chromatography.

4.2. General Instrumental Methods. UV−visible spectra were recorded on an HP 8453 spectrophotometer. ^{1}H NMR spectra were recorded on a 400 MHz Bruker AVANCE III HD spectrometer equipped with a 5 mm BB/1H SmartProbe and a 600 MHz Bruker AVANCE III HD equipped with a 5 mm inverse triple resonance TCI cryoprobe (^{1}H/^{13}C/^{15}N/^{2}H) with cooled pre-amplifiers for ^{1}H, ^{13}C, and ^{2}H and referenced to residual $CHCl_3$ at 7.26 ppm (or to residual benzene at 7.16 ppm and residual DMSO at 2.5 ppm). HR-ESI mass spectra were recorded on an LTQ Orbitrap XL spectrometer, using methanolic solutions and typically in the positive ion mode.

Cyclic voltammetry was carried out at 298 K with an EG&G model 263A potentiostat equipped with a three-electrode system: a glassy carbon working electrode, a platinum wire counter electrode, and a saturated calomel reference electrode (SCE). Tetra(*n*-butyl)ammonium perchlorate, recrystallized twice from absolute ethanol and dried in a desiccator for at least 2 weeks, was used as the supporting electrolyte. Anhydrous CH_2Cl_2 (Aldrich) was used as the solvent. The reference electrode was separated from the bulk solution by a fritted-glass bridge filled with the solvent/supporting electrolyte mixture. The electrolyte solution was purged with argon for at least 2 min prior to all measurements, which were carried out under an argon blanket. All potentials were referenced to the SCE.

5. SYNTHETIC METHODS

5.1. H_3[AzuC]. To a solution of azulene (186.2 mg, ∼1, 5 mmol) in a mixture of pyrrole (313 μL, 4.5 mmol) and 4-trifluoromethylbenzaldehyde (342 μL, 2.5 mmol) was added a solution of 10% TFA in dichloromethane (40 μL). After stirring at room temperature for 1 h, the mixture was dissolved in dichloromethane (50 mL), quenched with DDQ (337.8 mg, ∼1.5 mmol) dissolved in tetrahydrofuran (10 mL), and stirred for an additional 0.5 h. The reaction mixture was then washed in a separatory funnel with aqueous sodium chloride and back-extracted with chloroform until the aqueous phase was no longer yellow. The combined organic phases were rotary-evaporated to dryness and the residue was chromatographed on a basic alumina column starting with 9:1 pentane/dichloromethane as the eluent. The polarity of the eluent was gradually increased until a green fraction was collected with 3:1 pentane/dichloromethane and evaporated to dryness.[37,38] The resulting solid upon washing with a minimum amount of pentane yielded pure H_3[AzuC] as a dark bluish-green solid. Yield: 3.9 mg (0.34% relative to azulene). UV−vis (CH_2Cl_2) λ_{max} (nm), $\epsilon \times 10^{-4}$ (M^{-1} cm^{-1}): 375 (3.73), 478 (2.64), 503 (2.45), 628 (1.91); UV−vis (CH_2Cl_2 + 1% TFA) λ_{max} (nm), $\epsilon \times 10^{-4}$ (M^{-1} cm^{-1}): 399 (4.02), 522 (3.33), 639 (2.07), 857 (1.78). ^{1}H NMR (600 MHz, $CDCl_3$, δ; see Scheme 1 for atom numbering): δ 9.30 (d, J = 9.7 Hz, 1H, azulene-2^1), 8.07 (d, J = 7.8 Hz, 2H, 5-*o*-Ph), 8.01 (d, J = 7.8 Hz, 2H, 15-*o*-Ph), 7.95 (d, J = 3.9 Hz, 1H, β-H), 7.94−7.89 (m, 3H, overlapping 5-*m*-Ph and β-H), 7.88 (d, J = 7.9 Hz, 2H, 15-*m*-Ph), 7.86−7.80 (m, 5H, overlapping 10-*o*-Ph, 10-*m*-Ph and azulene-3^1), 7.64 (d, J = 4.5 Hz, 1H, β-H), 7.61−7.56 (m, 2H, overlapping β-H and azulene-2^3), 7.45−7.39 (m, 2H, overlapping β-H and azulene-2^2), 7.21 (d, J = 4.5 Hz, 1H, β-H), 7.09 (t, J = 9.9 Hz, 1H, azulene-3^2), 3.47 (s, 1H, core NH), 3.19 (s, 1H, core CH). ^{1}H NMR (400 MHz, C_6D_6, δ): 8.97 (d, J = 9.4 Hz, 1H, azulene-2^1), 7.81−7.76 (m, 3H), 7.74 (d, J = 3.9 Hz, 1H, β-H), 7.70−7.60 (m, 8H), 7.59−7.52 (m, 5H), 7.38 (d, J = 4.6 Hz, 1H, β-H), 7.27 (d, J = 5.3 Hz, 1H, β-H), 6.81 (t, J = 9.5 Hz, 1H, azulene), 6.74 (t, J = 9.5 Hz, 1H, azulene), 6.29 (t, J = 9.7 Hz, 1H, azulene), 3.45 (s, 1H, core NH), 3.09 (s, 1H, central CH). ^{1}H NMR (400 MHz, DMSO-d_6, δ): 9.51 (d, J = 9.8 Hz, 1H, azulene-2^1), 8.30−8.25 (m, 1H), 8.20−8.10 (m, 3H), 8.10−8.00 (m, 6H), 7.99−7.87 (m, 4H), 7.82−7.72 (m, 2H), 7.68−7.58 (m, 3H), 7.42 (d, J = 4.9 Hz, 1H, β-H), 7.29 (t, J = 9.8 Hz, 1H, azulene), 7.16 (d, J = 5.1 Hz, 1H, β-H). ESI-MS m/z: calcd for $C_{46}H_{26}N_3F_9H$, 792.2067 [M + H^+]; found, 792.2033.

5.2. Cu[AzuC]. Free-base H_3[AzuC] (2.2 mg) and $Cu(OAc)_2 \cdot H_2O$ (1 equiv) were dissolved in pyridine (10 mL) and stirred for 1 h. The solvent was removed under vacuum and the residue was chromatographed on a silica gel column with 5:1 pentane/dichloromethane as the eluent. The first green fraction was collected and evaporated to dryness.

DOI: 10.1021/acsomega.9b00275
ACS Omega 2019, 4, 6737−6745

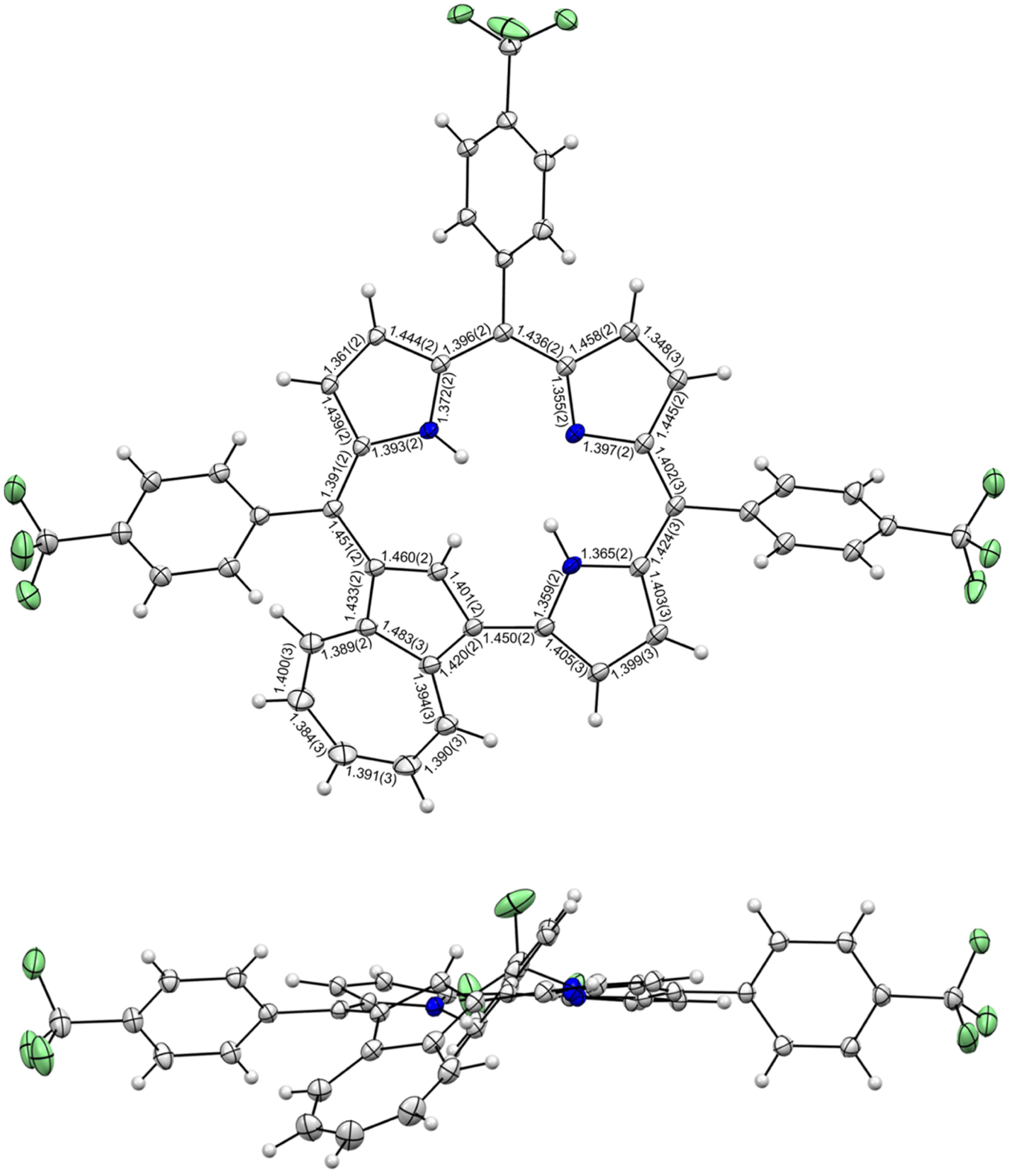

Figure 2. Thermal ellipsoid plots (50%) of H_3[AzuC]: top view (above), including selected skeletal bond distances (Å), and side view (below).

The residue upon washing with methanol yielded pure Cu[AzuC] as a bright-green solid. Yield 2.1 mg (88.7%). UV−vis (CH_2Cl_2) λ_{max} (nm), [$\varepsilon \times 10^{-4}$ (M^{-1} cm^{-1})]: 385 (1.73), 430 (1.12), 453 (1.26), 494 (1.04), 614 (1.50), 753 (0.16). ^{1}H NMR (400 MHz, $CDCl_3$, δ): 9.15 (d, J = 9.8 Hz, 1H, azulene-2^1), 8.19 (d, J = 4.3 Hz, 1H, β-H) 8.11 (d, J = 7.9 Hz, 2H, 10/15-*o*-Ph), 7.99 (d, J = 7.9 Hz, 2H, 5/10/15-*o*-Ph), 7.97−7.92 (m, 5H, overlapping β-H and Ph), 7.90 (d, J = 8.4 Hz, 2H, 5/10/15-*m*-Ph), 7.88 (d, J = 8.1 Hz, 2H, 5/10/15-*m*-Ph), 7.84 (d, J = 9.6 Hz, 1H, azulene-3^1), 7.74−7.71 (m, 2H, overlapping β-H), 7.66 (d, J = 5.2 Hz, 1H, β-H), 7.59−7.51 (m, 2H, overlapping β-H and azulene-2^3), 7.43 (t, J = 9.5 Hz, 1H, azulene-2^2), 7.05 (t, J = 9.9 Hz, 1H, azulene-3^2). MS (ESI)

DOI: 10.1021/acsomega.9b00275
ACS Omega 2019, 4, 6737−6745

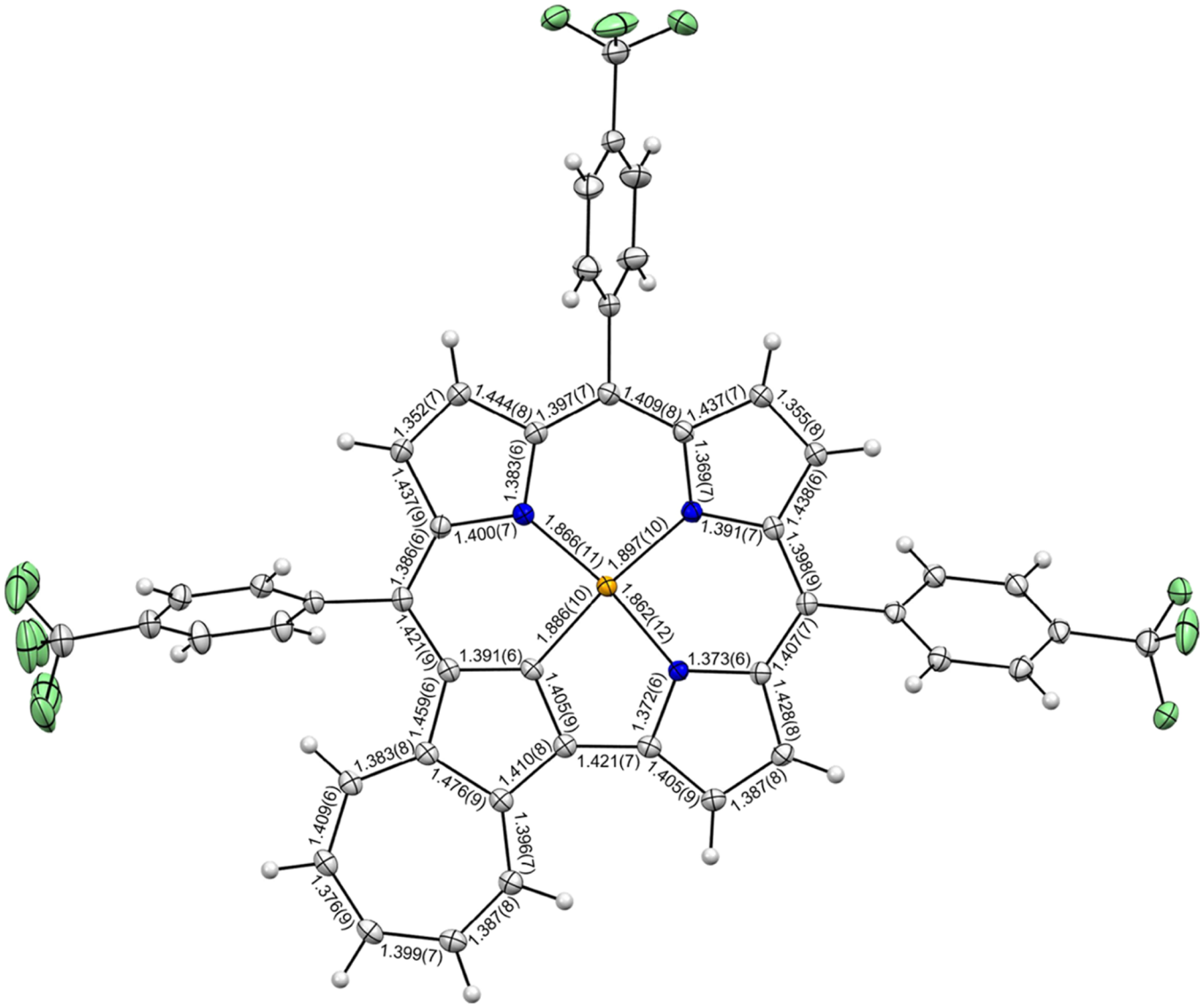

Figure 3. Thermal ellipsoid plot (50%) of Cu[AzuC].

Scheme 2. Dipolar Resonance Form of H_3[AzuC]

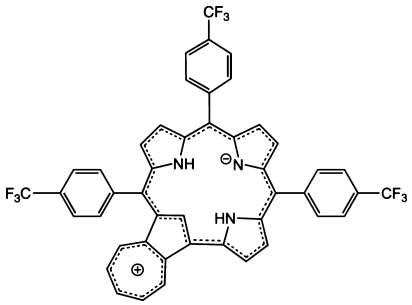

m/*z*: calcd for $C_{46}H_{23}N_3F_9Cu$, 851.1050 [M^+]; found, 851.1031.

5.3. Au[AzuC]. Free-base H_3[AzuC] (9.3 mg) and $Au(OAc)_3$ (5 equiv) were dissolved in pyridine (10 mL) and stirred overnight. The solvent was removed under vacuum and the residue was chromatographed on a silica gel column with 5:1 pentane/dichloromethane as the eluent. The first green fraction was collected and evaporated to dryness. The residue upon washing with methanol yielded pure Au[AzuC] as a bright-green solid. Yield 3.7 mg (32.0%). UV−vis (CH_2Cl_2) λ_{max} (nm), [$\epsilon \times 10^{-4}$ (M^{-1} cm^{-1})]: 351 (0.62), 382 (0.69), 399 (0.73), 450 (0.54), 499 (0.46), 610 (0.40), 761 (0.11), 837 (0.08). ^{1}H NMR (400 MHz, $CDCl_3$, δ): 9.00 (d, J = 9.9 Hz, 1H, azulene-2^1), 8.15−8.09 (m, 3H, overlapping β-H and

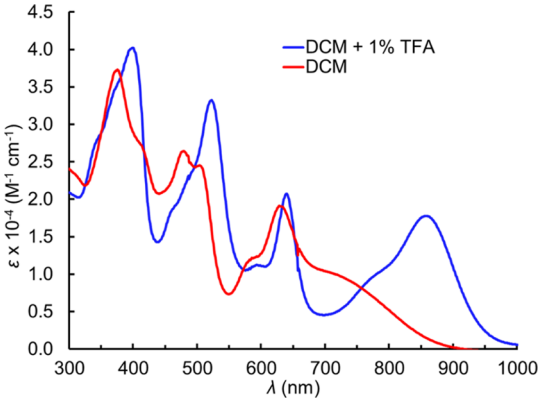

Figure 4. UV−visible−NIR spectra of H_3[AzuC] in dichloromethane with and without 1% TFA.

DOI: 10.1021/acsomega.9b00275
ACS Omega 2019, 4, 6737−6745

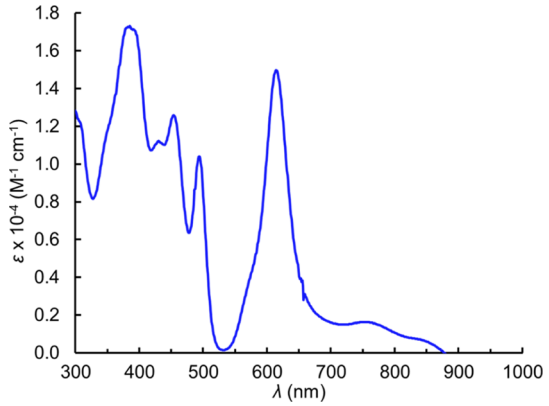

Figure 5. UV−vis−NIR spectrum of Cu[AzuC] in dichloromethane.

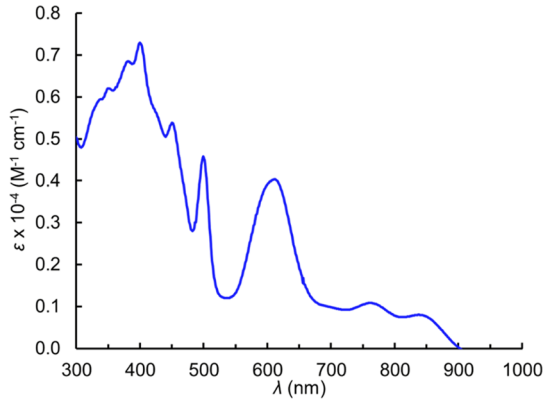

Figure 6. UV−vis−NIR spectrum of Au[AzuC] in dichloromethane.

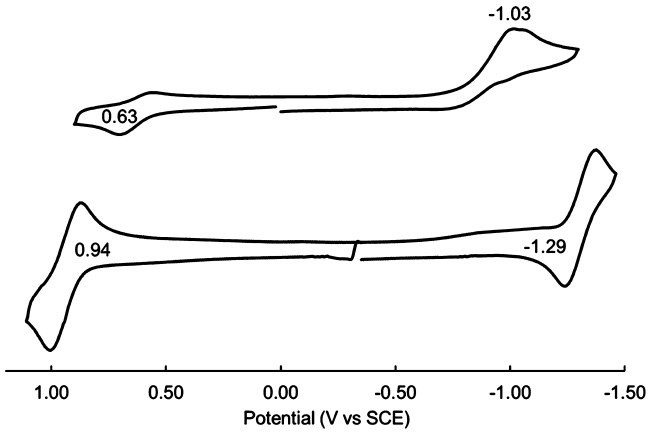

Figure 7. CV of Au[AzuP] (top) and the analogous Au *meso*-tris(4-trifluoromethylphenyl)corrole (bottom) in CH_2Cl_2 containing 0.1 M TBAP. Scan rate = 100 mV/s.

10-*o*-Ph), 8.00 (d, J = 8.0 Hz, 2H, 5/15-*o*-Ph), 7.97 (d, J = 8.2 Hz, 2H, 5/15-*o*-Ph), 7.94 (d, J = 8.3 Hz, 2H, 10-*m*-Ph), 7.93−7.89 (m, 4H, overlapping 5-*m*-Ph and 15-*m*-Ph), 7.88 (d, J = 3.2 Hz, 1H, β-H), 7.74−7.71 (m, 3H, overlapping β-H), 7.66−7.62 (m, 2H, overlapping β-H and azulene-3[1]), 7.49 (t, J = 9.5 Hz, 1H, azulene-2[3]), 7.39 (t, J = 9.5 Hz, 1H, azulene-2[2]), 6.97 (t, J = 9.3 Hz, 1H, azulene-3[2]). MS (ESI) m/z: calcd for $C_{46}H_{23}N_3F_9Au$, 985.1419 [M^+]; found, 985.1374.

5.4. X-ray Structure Determination. Suitable crystals were obtained by diffusion of methanol vapor into a concentrated solution of H_3[AzuC] in benzene and Cu[AzuC]

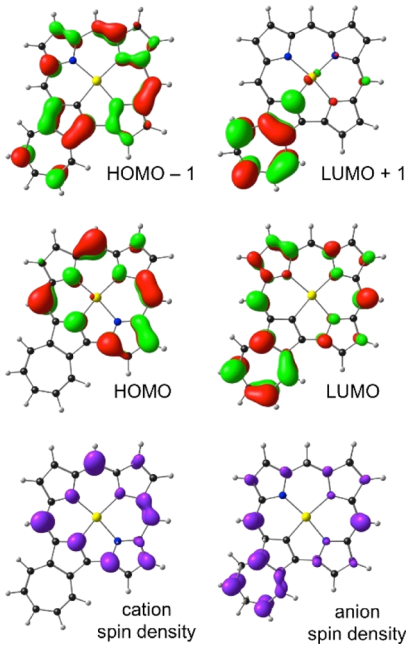

Figure 8. Selected MO and spin density plots for Au[AzuC].

in toluene. X-ray data were collected on beamline 12.2.1 at the Advanced Light Source of Lawrence Berkeley National Laboratory, Berkeley, California. The samples were mounted on MiTeGen kapton loops and placed in a 100(2) K nitrogen cold stream provided by an Oxford Cryostream 700 Plus low-temperature apparatus on the goniometer head of a Bruker D8 diffractometer equipped with a PHOTON II CPAD detector. Diffraction data were collected using synchrotron radiation monochromated with silicon (111) to a wavelength of 0.7288(1) Å. In each case, an approximate full-sphere of data was collected using 1° ω scans. Absorption corrections were applied using SADABS.[39] The structure was solved by intrinsic phasing (SHELXT)[40] and refined by full-matrix least squares on F^2 (SHELXL-2014)[41] using the ShelXle GUI.[42] Appropriate scattering factors were applied using the XDISP[43] program within the WinGX suite.[44] All non-hydrogen atoms were refined anisotropically. Hydrogen atoms were geometrically calculated and refined as riding atoms.

■ ASSOCIATED CONTENT

Supporting Information

The Supporting Information is available free of charge on the ACS Publications website at DOI: 10.1021/acsomega.9b00275.

^{1}H NMR spectrum of H_3[AzuC] in $CDCl_3$ and the inset displays core protons. ^{1}H NMR spectrum of H_3 [AzuC] in benzene-d_6 and the inset displays core protons; ^{1}H NMR spectrum of H_3[AzuC] in DMSO-d_6; NOESY of H_3[AzuC] in $CDCl_3$; TOCSY of H_3[AzuC] in $CDCl_3$; ^{1}H NMR spectrum of Cu[AzuC] in $CDCl_3$; NOESY of Cu[AzuC] in $CDCl_3$; TOCSY of Cu[AzuC] in $CDCl_3$; ^{1}H NMR spectrum of Au[AzuC] in $CDCl_3$; NOESY of Au[AzuC] in $CDCl_3$; TOCSYof Au[AzuC] in $CDCl_3$; ESI-MS spectrum of H_3[AzuC]; ESI-MS spectrum of Cu[AzuC]; and ESI-MS spectrum of Au[AzuC] (PDF)

Crystallographic Data for H_3[AzuC] (CIF)

Crystallographic Data for Cu[AzuC] (CIF)

DOI: 10.1021/acsomega.9b00275
ACS Omega 2019, 4, 6737−6745

Accession Codes

The crystal structures referred to herein have been deposited to the Cambridge Structural Database and assigned the deposition numbers CCDC 1893183−1893184.

AUTHOR INFORMATION

Corresponding Author

*E-mail: abhik.ghosh@uit.no. Twitter: @abhikghosh. Phone: +47 45476145.

ORCID

Laura J. McCormick-McPherson: 0000-0002-6634-4717

Abhik Ghosh: 0000-0003-1161-6364

Notes

The authors declare no competing financial interest.

ACKNOWLEDGMENTS

This work was supported by grant 262229 of the Research Council of Norway and by the Advanced Light Source, Berkeley, California. The Advanced Light Source is supported by the Director, Office of Science, Office of Basic Energy Sciences, of the U.S. Department of Energy under contract no. DE-AC02-05CH11231.

REFERENCES

(1) Furuta, H.; Maeda, H.; Osuka, A. Confusion, inversion, and creation-a new spring from porphyrin chemistry. *Chem. Commun.* **2002**, 1795−1804.

(2) Ghosh, A. A Perspective of One-Pot Pyrrole-Aldehyde Condensations as Versatile Self-Assembly Processes. *Angew. Chem., Int. Ed.* **2004**, *43*, 1918−1931.

(3) Orłowski, R.; Gryko, D.; Gryko, D. T. Synthesis of Corroles and Their Heteroanalogs. *Chem. Rev.* **2017**, *117*, 3102−3137.

(4) Lash, T. D.; Colby, D. A.; Ferrence, G. M. Further Studies on the Synthesis ofmeso-Tetraarylazuliporphyrins under Lindsey−Rothemund Reaction Conditions and Their Conversion into Benzocarbaporphyrins. *Eur. J. Org. Chem.* **2003**, 4533−4548.

(5) Colby, D. A.; Lash, T. D. Adaptation of the Rothemund Reaction for Carbaporphyrin Synthesis: Preparation of meso-Tetraphenylazuliporphyrin and Related Benzocarbaporphyrins. *Chem.—Eur. J.* **2002**, *8*, 5397−5402.

(6) Lindsey, J. S.; Schreiman, I. C.; Hsu, H. C.; Kearney, P. C.; Marguerettaz, A. M. Rothemund and Adler-Longo reactions revisited: synthesis of tetraphenylporphyrins under equilibrium conditions. *J. Org. Chem.* **1987**, *52*, 827−836.

(7) Lindsey, J. S.; Hsu, H. C.; Schreiman, I. C. Synthesis of Tetraphenylporphyrins under Very Mild Conditions. *Tetrahedron Lett.* **1986**, *27*, 4969−4970.

(8) Chmielewski, P. J.; Latos-Grażyński, L. Core modified porphyrins - a macrocyclic platform for organometallic chemistry. *Coord. Chem. Rev.* **2005**, *249*, 2510−2533.

(9) Lash, T. D. Out of the Blue! Azuliporphyrins and Related Carbaporphyrinoid Systems. *Acc. Chem. Res.* **2016**, *49*, 471−482.

(10) Pawlicki, M.; Latos-Grażyński, L. Carbaporphyrinoids - Synthesis and Coordination Properties. In *Handbook of Porphyrin Science: With Applications to Chemistry, Physics, Materials Science, Engineering, Biology and Medicine*; Kadish, K. M., Smith, K. M., Guilard, R., Eds.; World Scientific: Singapore, 2010; Vol. 2, Chapter 8, pp 104−192.

(11) Lash, T. D. Carbaporphyrinoid Systems. *Chem. Rev.* **2017**, *117*, 2313−2446.

(12) Ghosh, A. Electronic Structure of Corrole Derivatives: Insights from Molecular Structures, Spectroscopy, Electrochemistry, and Quantum Chemical Calculations. *Chem. Rev.* **2017**, *117*, 3798−3881.

(13) Fujino, K.; Hirata, Y.; Kawabe, Y.; Morimoto, T.; Srinivasan, A.; Toganoh, M.; Miseki, Y.; Kudo, A.; Furuta, H. Confusion and Neo-Confusion: Corrole Isomers with an NNNC Core. *Angew. Chem., Int. Ed.* **2011**, *50*, 6855−6859.

(14) The possible existence of azulicorrole has only been theoretically considered: Ghosh, A.; Larsen, S.; Conradie, J.; Foroutan-Nejad, C. Local versus global aromaticity in azuliporphyrin and benziporphyrin derivatives. *Org. Biomol. Chem.* **2018**, *16*, 7964−7970.

(15) Gryko, D. T.; Koszarna, B. Refined methods for the synthesis of *meso*-substituted A_3- and *trans*-A_2B-corroles. *Org. Biomol. Chem.* **2003**, *1*, 350−357.

(16) The use of azulene−carbinols was precluded by the fact that acid-catalyzed interaction of azulene and aldehydes results in immediate formation of calix[4]azulenes.

(17) Georghiou, P. E.; Rahman, S.; Alodhayb, A.; Nishimura, H.; Lee, J.; Wakamiya, A.; Scott, L. T. Calixazulenes: azulene-based calixarene analogues - an overview and recent supramolecular complexation studies. *Beilstein J. Org. Chem.* **2018**, *14*, 2488−2494.

(18) Bröring, M.; Brégier, F.; Cónsul Tejero, E.; Hell, C.; Holthausen, M. C. Revisiting the Electronic Ground State of Copper Corroles. *Angew. Chem., Int. Ed.* **2007**, *46*, 445−448.

(19) Alemayehu, A. B.; Gonzalez, E.; Hansen, L. K.; Ghosh, A. Copper Corroles Are Inherently Saddled. *Inorg. Chem.* **2009**, *48*, 7794−7799.

(20) Alemayehu, A. B.; Hansen, L. K.; Ghosh, A. Nonplanar, Noninnocent, and Chiral: A Strongly Saddled Metallocorrole. *Inorg. Chem.* **2010**, *49*, 7608−7610.

(21) Thomas, K. E.; Conradie, J.; Hansen, L. K.; Ghosh, A. A Metallocorrole with Orthogonal Pyrrole Rings. *Eur. J. Inorg. Chem.* **2011**, 1865−1870.

(22) Berg, S.; Thomas, K. E.; Beavers, C. M.; Ghosh, A. Undecaphenylcorroles. *Inorg. Chem.* **2012**, *51*, 9911−9916.

(23) Thomas, K. E.; McCormick, L. J.; Carrié, D.; Vazquez-Lima, H.; Simonneaux, G.; Ghosh, A. Halterman Corroles and Their Use as a Probe of the Conformational Dynamics of the Inherently Chiral Copper Corrole Chromophore. *Inorg. Chem.* **2018**, *57*, 4270−4276.

(24) Thomassen, I. K.; MCormick, L. J.; Ghosh, A. Synthesis and Molecular Structure of a Copper Octaiodocorrole. *ACS Omega* **2018**, *3*, 5106−5110.

(25) Maurya, Y. K.; Noda, K.; Yamasumi, K.; Mori, S.; Uchiyama, T.; Kamitani, K.; Hirai, T.; Ninomiya, K.; Nishibori, M.; Hori, Y.; Shiota, Y.; Yoshizawa, K.; Ishida, M.; Furuta, H. Ground-State Copper(III) Stabilized by *N*-Confused/*N*-Linked Corroles: Synthesis, Characterization, and Redox Reactivity. *J. Am. Chem. Soc.* **2018**, *140*, 6883−6892.

(26) Alemayehu, A. B.; Ghosh, A. Gold corroles. *J. Porphyrins Phthalocyanines* **2011**, *15*, 106−110.

(27) Rabinovich, E.; Goldberg, I.; Gross, Z. Gold(I) and Gold(III) Corroles. *Chem. - Eur. J.* **2011**, *17*, 12294−12301.

(28) Thomas, K. E.; Alemayehu, A. B.; Conradie, J.; Beavers, C.; Ghosh, A. Synthesis and Molecular Structure of Gold Triarylcorroles. *Inorg. Chem.* **2011**, *50*, 12844−12851.

(29) Thomas, K. E.; Vazquez-Lima, H.; Fang, Y.; Song, Y.; Gagnon, K. J.; Beavers, C. M.; Kadish, K. M.; Ghosh, A. Ligand Noninnocence in Coinage Metal Corroles: A Silver Knife-Edge. *Chem.—Eur. J.* **2015**, *21*, 16839−16847.

(30) Thomas, K. E.; Gagnon, K. J.; MCormick, L. J.; Ghosh, A. Molecular structure of gold 2,3,7,8,12,13,17,18-octabromo-5,10,15-tris(4′-pentafluorosulfanylphenyl)corrole: Potential insights into the insolubility of gold octabromocorroles. *J. Porphyrins Phthalocyanines* **2018**, *22*, 596−601.

(31) Wasbotten, I. H.; Wondimagegn, T.; Ghosh, A. Electronic Absorption, Resonance Raman, and Electrochemical Studies of Planar and Saddled Copper(III)meso-Triarylcorroles. Highly Substituent-Sensitive Soret Bands as a Distinctive Feature of High-Valent Transition Metal Corroles. *J. Am. Chem. Soc.* **2002**, *124*, 8104−8116.

(32) Gouterman, M.; Wagnière, G. H.; Snyder, L. C. Spectra of Porphyrins. *J. Mol. Spectrosc.* **1963**, *11*, 108−127.

DOI: 10.1021/acsomega.9b00275
ACS Omega 2019, 4, 6737−6745

(33) Gouterman, M. Optical Spectra and Electronic Structure of Porphyrins and Related Rings. In *The Porphyrins*; Dolphin, D., Ed.; Academic Press: New York, 1978; Vol. *III*, Part A, pp 1−165.
(34) Ghosh, A.; Wondimagegn, T.; Parusel, A. B. J. Electronic Structure of Gallium, Copper, and Nickel Complexes of Corrole. High-Valent Transition Metal Centers versus Noninnocent Ligands. *J. Am. Chem. Soc.* **2000**, *122*, 5100−5104.
(35) Alemayehu, A. B.; Day, N. U.; Mani, T.; Rudine, A. B.; Thomas, K. E.; Gederaas, O. A.; Vinogradov, S. A.; Wamser, C. C.; Ghosh, A. Gold Tris(carboxyphenyl)corroles as Multifunctional Materials: Room Temperature Near-IR Phosphorescence and Applications to Photodynamic Therapy and Dye-Sensitized Solar Cells. *ACS Appl. Mater. Interfaces* **2016**, *8*, 18935−18942.
(36) Teo, R. D.; Hwang, J. Y.; Termini, J.; Gross, Z.; Gray, H. B. Fighting Cancer with Corroles. *Chem. Rev.* **2017**, *117*, 2711−2729.
(37) Three fractions were collected and mass-spectrometrically analyzed prior to the azulicorrole fraction. The first of these consisted of unreacted azulene (36.4 mg, 19.5%). The second fraction consisted of oligomers containing 2 azulene units, 2 aldehyde units and one pyrrole (17 mg, 3.7% based on azulene). The third fraction consisted of 3 azulene units and 2 aldehyde units (5.7 mg, 1.2% based on azulene).
(38) The azulicorrole fraction was followed by regular corrole, whose yield hovered around 15% (based on pyrrole).
(39) Krause, L.; Herbst-Irmer, R.; Sheldrick, G. M.; Stalke, D. Comparison of silver and molybdenum microfocus X-ray sources for single-crystal structure determination. *J. Appl. Crystallogr.* **2015**, *48*, 3−10.
(40) Sheldrick, G. M. SHELXT- Integrated space-group and crystal-structure determination. *Acta Crystallogr.* **2015**, *71*, 3−8.
(41) Sheldrick, G. M. Crystal structure refinement withSHELXL. *Acta Crystallogr.* **2015**, *71*, 3−8.
(42) Hübschle, C. B.; Sheldrick, G. M.; Dittrich, B. ShelXle: a Qt graphical user interface forSHELXL. *J. Appl. Crystallogr.* **2011**, *44*, 1281−1284.
(43) Kissel, L.; Pratt, R. H. Corrections to tabulated anomalous-scattering factors. *Acta Crystallogr.* **1990**, *46*, 170−175.
(44) Farrugia, L. J. WinGXandORTEP for Windows: an update. *J. Appl. Crystallogr.* **2012**, *45*, 849−854.

DOI: 10.1021/acsomega.9b00275
ACS Omega 2019, 4, 6737−6745